Journal of Physics: Conference Series

Large eddy simulation with realistic geophysical inflow of Alpha Ventus wind farm: a comparison with LIDAR field experiments

To cite this article: Tanmoy Chatterjee *et al* 2018 *J. Phys.: Conf. Ser.* **1037** 072056

Large eddy simulation with realistic geophysical inflow of Alpha Ventus wind farm: a comparison with LIDAR field experiments

Tanmoy Chatterjee, Nihanth Wagmi Cherukuru, Yulia T. Peet and Ronald J. Calhoun

SEMTE, Arizona State University, Tempe, AZ-85287, US

Abstract. In the current paper we perform a high Reynolds number large eddy simulation (LES) study of the offshore Alpha Ventus wind farm in North Sea. Actuator line modeling has been used for the rotating turbines. The wind farm is driven by a neutral atmospheric boundary layer coupled with realistically varying mean wind flux and direction from cup and vane anemometer data. We carry out comparison of LES and LIDAR based experimental results obtained from low-elevation angle Plan Position Indicator (PPI) scans of the velocity structures between two turbines. The results indicate towards a more fundamental understanding on the capability of LES inflow methodology in capturing realistic large scale structures that are observed in wind farm flows.

1. Introduction

The wake interactions in the downstream turbines and the power generated by the wind turbines in massive wind farms depend significantly on the turbulent inflow wind conditions from the atmospheric boundary layer (ABL) [1, 2, 3]. Many computational and laboratory studies involving flow past wind farms assume constant mean wind speed and wind direction neglecting large scale geophysical effects [4, 5, 6, 7]. These effects are important for wind farm performance and hence studies in the past have attemped to bridge the gap by performing the wind farm simulations driven by realistic winds from data assimilation coupled with the Weather Research and Forecast (WRF) model [8, 9]. WRF models utilized are usually driven by data assimilation methodologies [8, 9]. In several of these studies, field experimental results from remote sensing LIDAR scans have been used for comparison. For example, [10] performed Reynolds-Averaged Navier Stokes (RANS) simulation on a complex terrain driven by mesoscale WRF. Further, [11] have investigated the wake evolution of turbines under different atmospheric stability conditions in a nested large eddy simulation (LES) of finer grids around the wind turbine model, inside a coarser LES mesh driving precursor ABL coupled with weather forecast model. The results have been compared against the vertical profiling of LIDAR data involving dual LIDAR scans. However, the computational expense for these nested LES models (interpolation from the coarse mesh to the finer mesh for all the interior domain boundaries) is extremely high if a large wind farm domain with varying mean wind directions are used. [11] attempts to ameliorate this computational bottleneck, by performing nested simulations for a single wind turbine. A more recent study [12] attempts to evaluate RANS and Detatched-Eddy Simulation (DES) in complex terrain with the LIDAR measurements. The computational results have indicated some prediction of the trends of the velocity and turbulent stresses with a reasonable amount of scatter.

In this context, our previous study [13] as a computationally inexpensive alternative has incorporated geophysical effects of varying mean wind flux and mean direction from the cup and vane anemometer data into an LES framework. The study has revealed that these large scale effects can have significant impact on the power generated by the wind farms.

Although presenting a methodology for incorporating large scale geophysical effects into the LES simulations, our previous work [13] did not provide a comparison of the wind turbine wakes with the field data. In the current paper, our focus is on the comparison of the wind turbine wakes obtained with a similar mean wind based data-driven methodology, with the velocity measurements downstream of wind turbines. The single LIDAR measurements are taken at the off-shore wind farm called Alpha Ventus located in the North Sea by the Environmental Remote Sensing group at Arizona State University. The LES results are compared against these 2D VAR retrieved LIDAR scans. The objective of the current work lies in understanding the capability of the present LES methodology fed by the mean wind information in capturing the realistic large scale structures observed in the field experiments.

In the current paper, comparison of the temporally filtered LES velocity fields as well as time variation of the spatially filtered fields in the location between two turbines with that of the LIDAR experimental scan have been carried out. The physical consistency of the simulation results for the current domain has been tested with the spatial energy spectra which indicates the presence of the $-5/3$ law in accordance with the Kolmogorov turbulence cascade.

2. Computational Setup

Wind Turbine	N_t	z_h	D	Ω	rated power	rated wind speed
Adwen AD 5-116	3×2	90 m	116 m	5.9 – 14.0 rpm	5 MW	12.5 m/s
Senvion 5M	3×2	92 m	126 m	6.9 – 13.1 rpm	5 MW	13.0 m/s

Table 1: Turbines in Alpha Ventus wind farm. N_t – the number of turbines, D – turbine rotor diameter, z_h– wind turbine hub-height. Ω – speed of the rotation of the turbine rotor. Turbines T3,T7,T11,T4,T8,T12 – Senvion 5M turbines, T1,T5,T9,T2,T6,T10 – Adwen AD 5-116 turbines.

Case	Geometry	$N_x^e \times N_y^e \times N_z^e$	Grid points
precursor ABL	$54D \times 27D \times 8.6D$ (6.2 km × 3.1 km × 1 km)	$30 \times 24 \times 20$	5.03×10^6
WT array	$54D \times 21D \times 8.6D$ (6.2 km × 2.4 km × 1 km)	$46 \times 24 \times 40$	1.53×10^7

Table 2: Computational domain size (normalized with turbine rotor diameter and also in kilometres) and grid-requirements for ABL & wind turbine array computational domain. 7^{th} order Legendre polynomial has been used per cartesian direction to expand variables in each spectral element. Domain normalized with D, the diameter of Adwen AD 5-116 turbines.

The computational domain comprises of the wind turbine array containing 12 turbines (arranged as in the Alpha Ventus wind farm) and is set up with an inflow-outflow boundary conditions in the streamwise direction using higher order exponentially accurate spectral element solver `Nek5000`.

Both the precursor and the wind turbine array domain are simulated in an LES with near-wall modeling framework at Reynolds number $Re = U_\infty H/\nu \sim 10^{10}$ [14] (U_∞ is the time averaged mean free-stream velocity of the precursor ABL, H is the ABL thickness, ν, molecular viscosity, which is roughly 5 orders of magnitude lower than the subgrid scale viscosity). The setup is very similar in spirit with the hybrid RANS-LES methodology [15], with the near-wall eddy viscosity

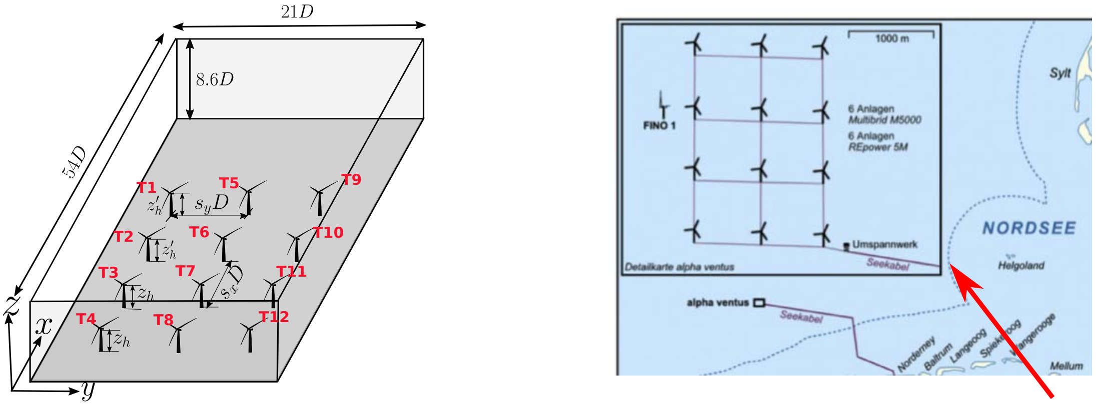

(a) (b)

Figure 1: (a) Computational domain to simulate realistic flow past the 12 turbines in Alpha Ventus farm. (b) Location of the wind farm at North Sea: Red arrow – direction of dominant wind.

coefficient analogous to the RANS based mixing length model correponding to the log-layer independent of the grid size scaling. The methodology is justified as opposed to a complete RANS model beyond its capability in comparing against the trends of the LIDAR field data, i.e. understanding the realistic high *Re* turbulence, its spectral characteristics in future. The rotating turbine blades have been modeled using "actuator lines" [16, 17] with a constant tip speed ratio, = 4.6 (Adwen turbines), = 5.0 (Senvion turbines), corresponding to their rated wind speed and the rotational speed of the rotor. For precursor simulation, periodic boundary conditions have been used in the streamwise and spanwise directions, while shear stress and stress free boundaries have been used in the bottom and top boundary planes respectively.The precusor ABL is essentially modeled as an open channel flow without the Coriolis forces and the capping inversion [14], but capable of reproducing the inner and outer layer physics in terms of the log-law of the wall, spectra, and integral length scales. The boundary conditions for the wind farm domain remains the same as the precursor ABL, except in the streamwise direction where the inflow-outflow methodology has been used [16, 13]. The inflow is driven by a precursor neutrally-stratified ABL [14] with the temporal variation of mean wind flux and wind direction obtained from the data of cup and vane anemometer (CVA) located at the FINO platform (See Figure 1b). The details of the turbine configurations, e.g., the rotor size, hub-height and rated speed for the Alpha Ventus wind farm can be found in Table 1.

2.1. Incorporating mean wind flux and direction in LES

Incorporating the geophysical effect of the varying mean wind speed is implemented by changing the pressure gradient forcing through the Stokes solver in the preprocessor step. Note, this splitting scheme is applied only for the doubly periodic precursor simulation, where a forcing function is necessary to drive the flow. The precursor simulation is solved concurrently along with the wind turbine domain, which drives the flow past the array of turbines as inflow to the domain via spectral interpolation [16, 13].

The splitting scheme for the NS equation can be given as follows.

$$\mathfrak{L}_1(\mathbf{u}^{'}) + \mathfrak{L}_2(p^{'}) = \mathfrak{N}\mathfrak{L}(\mathbf{u}^{'}, \nabla\mathbf{u}^{'}) + B.C. \quad (1)$$

$$\mathfrak{L}_1(\mathbf{u}_0) + \mathfrak{L}_2(p_0) = \mathbf{f}_0 + B.C.(0) \quad (2)$$

where the linear operators, $\mathfrak{L}_1 = \partial/\partial t - (\nu + \nu_t)\nabla^2$, $\mathfrak{L}_2 = 1/\rho\nabla$, and the non-linear operator

$\mathfrak{NL}(\mathbf{u}, \nabla\mathbf{u})$ have been used as compact notations for the corresponding NS operators. The reconstruction of the total NS variables at each timestep can be obtained as $[\mathbf{u}\ p\ \mathbf{f}] = [\mathbf{u}^{'}\ p'\ 0] + \alpha[\mathbf{u}_0\ p_0\ f_0]$. ν is the kinematic viscosity of the fluid, while ν_t is the LES filtering eddy viscosity based on Smagorinsky type of closure.

The forcing function $\mathbf{f}_0$ represents the time-invariant unit pressure gradient forcing corresponding to the homogeneous linear NS equation in Equation 1. BC in Equation 1 is the boundary condition for the 3D inhomogeneous problem. The homogeneous boundary condition $BC(0)$ for the linearized split NS equation (Equation 2), comprises of periodic boundary conditions in the streamwise and spanwise directions, while homogeneous Neumann type stress-free boundary conditions are implemented in the wall-normal direction. With flow-rate at time t, being $c(t)$, and A and V being the cross-sectional area of the flow and computational volume of the domain respectively and α being a free parameter, the time varying flow rate (fed from the cup and vane anemometer data at the bottom tip, and proportionately scaled for the bulk mean assuming logarithmic trends in the inner layer) can be written as

$$c(t) = \frac{A}{V}\int_{\Omega} \mathbf{u}\mathrm{d}\Omega = \frac{A}{V}\int_{\Omega}(\mathbf{u}^{'} + \alpha\mathbf{u}_0)\mathrm{d}\Omega \quad , \ \alpha(t) = \frac{(c(t) - \frac{A}{V}\int_{\Omega}\mathbf{u}^{'}\mathrm{d}\Omega)}{\frac{A}{V}\int_{\Omega}\mathbf{u}_0\mathrm{d}\Omega} \tag{3}$$

The variation in the wind direction (wind veering – geophysical effect) has been incorporated by rotating the precursor inflow along the lines of Munters et al. [2] but without using a domain-mapping methodology since the wind turbine domain inflow regime is completely overlapped by the precursor domain. Equation 4 shows the horizontal inlet velocities u_{inlet}, v_{inlet} obtained from the horizontal velocities u, v of the precursor ABL in the midplane, $x = \pi H$, with the mean wind direction $\theta_{mean}(t)$. At each timestep, the inflow domain is rotated by $\theta_m(t)$ about the point $[x_c, y_c]^T = [0, L_y/2]^T$ which serves as the center of rotation ($[-L_x/2\ L_x/2] \times [0\ L_y]$ is the extent of the precursor domain). The rotation matrix $\boldsymbol{R}(\theta(t))$ applied to the precursor domain coordinates and the horizontal velocities u, v can be given as

$$\boldsymbol{R}(\theta(t)) = \begin{bmatrix}\cos(\theta_m(t)) & -\sin(\theta_m(t))\\ \sin(\theta_m(t)) & \cos(\theta_m(t))\end{bmatrix}, \text{with} \begin{bmatrix}u_{inlet}\\ v_{inlet}\end{bmatrix} = \boldsymbol{R}\begin{bmatrix}u\\ v\end{bmatrix} \tag{4}$$

Here θ_m in Equation 4 is obtained from the mean wind direction data (Figure 2b). Due to the rotation of the precursor simulation, the data to inflow condition in the wind turbine array domain is being spectrally interpolated at each timestep from the precursor domain. Along the lines of Munters et al. [2], we can define a z dependant ratio $\varphi(z) = \frac{\Omega L_h}{U_h(z)}$, where $\Omega = d\theta_m/dt$ is the rotation rate of wind direction, $L_h = \sqrt{(L_{m,x}^2 + L_{m,y}^2)}$ is the horizontal diagonal of the main domain ($L_{m,x}$ and $L_{m,y}$ are the streamwise and spanwise extent of the main domain respectively) and $U_h(z)$ is the temporally and horizontally averaged mean velocity of the precursor domain. In this methodology, the timescale in the change of wind direction is significantly lower than the timescale imposed by the microscale turbulence, which is justified by the fact that our $\varphi \approx O(10^{-2})$ (upper bound $\varphi < 2/3$) ensuring that the artificial elongation and compression of the turbulent structures can be neglected.

2.2. A note on the spanwise periodicity in the wind turbine domain

In our computation, the inflow plane is spectrally interpolated from the streamwise location of the precursor ABL domain, while the spanwise boundary conditions are assumed periodic (wider spanwise extent with periodicity have been used in previous literatures [1, 18]). The design of the domain overlapping is done in such a manner that the precursor box rotates by approximately ≈ ±40° without leaving any inflow plane out of bounds with respect to the precursor domain. This approach in our two-domain LES simulations is offered as an attempt to a computationally

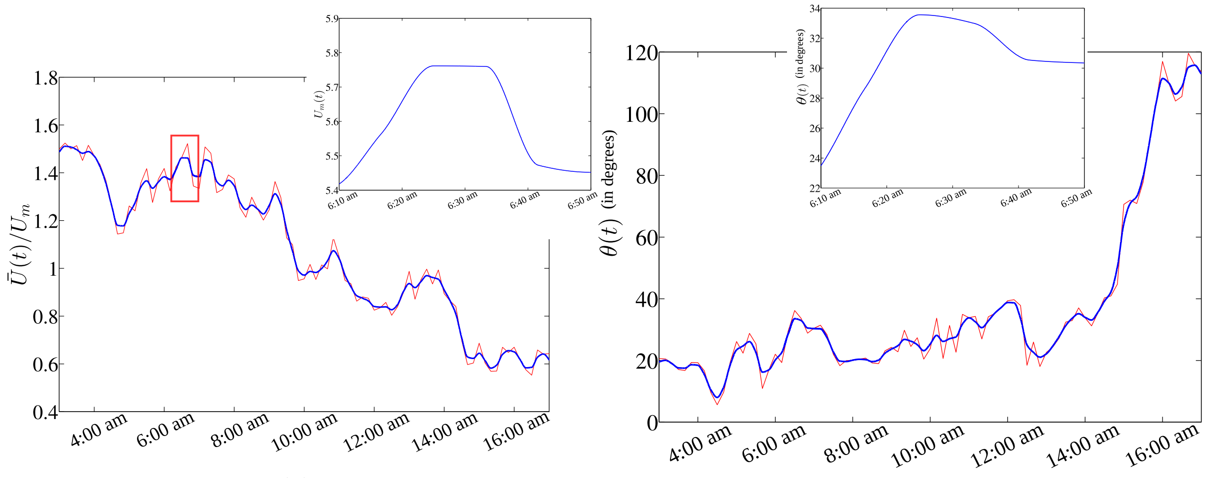

(a) (b)

Figure 2: Variation of (a) Mean wind velocity (b) Mean wind direction with time on 31st August 2016 collected by the cup and vane anemometer from the metereological mast around the bottom tip of the turbine at FINO platform. Red thin – mean from 10 minute averaged wind data interpolated using piecewise cubic Hermite polynomials corresponding to temporal LES resolution ($\Delta t \approx 0.06$ secs.). Blue thick – Gaussian smoothing performed on the 10 minute averaged wind using non-overlapping windowing involving 5 points. The red boxes indicate the data taken to feed our LES simulations for that particular exetent of time. Insets: zoomed-in fed mean wind velocity and wind direction data to simulations.

cheaper alternative to full-nested simulations [11] requiring a wider precursor domain or precusor rotation with domain mapping [19] (when the inflow plane is out of bounds due to precursor box rotation).

The spanwise periodic boundary condition gives rise to the locked-in large scale structures which are generally unavoidable and no effective solution has been found to deal with them, except perhaps with the shifted periodic boundary conditions as noted by Munters et al. [19] which were found to influence the spectral scaling of the turbulence at smaller scales, where Kolmogorov cascade is dominant. Studies involving data assimilation, where the spatio-temporal velocity data from the field experiments is coupled with the simulations, would still have these locked in features and hence need careful analysis. Furthermore, it must be noted that since locked-in structures are typically a large scale phenomenon, with length scales involving 5-10 times the domain size, significant increment of the domain size is required, which would create an extremely high computational overhead on the LES simulations. Despite being a large scale event, the locked in structures are local and are not known to influence the spatially averaged results or the two dimensional energy spectra. In addition, our spectral analysis (Figure 9) reveals that this methodology successfully captures the inertial range of turbulence in the streamwise and spanwise scales $\lesssim 5D$ as is evident in the Kolmogorov -5/3 cascade ($\lambda_{x,y}^{2/3}$ in premultiplied spectrum vs wavelengths).

Note that only one LIDAR (located in the FINO platform, See Figure 1b) has been used for low-elevation PPI scan. A LIDAR scan essentially is completed in 45 secs, but since multiple snaphot of raw LIDAR scans have been used in the 2D VAR optimization algorithm, the two retrived snapshots are usually 1-2 minutes apart. In the retrieval methodology, only the inplane velocities (i.e. in the plane scanned by the line of sight of LIDAR) have been considered. The mean wind speed and direction obtained from the LIDAR retrieval have been validated against the CVA data within 5% accuracy. Refer to [20] for more details regarding the 2D VAR algorithm and the LIDAR data retrieval.

It is also to be noted that the resolution of LES simulations of the WT array is $\sim 0.25D$ or 30 metres in the coarser regions of the mesh, while near the wind turbine array, it is around $0.04D$ or 5 metres. The LIDAR retrievals (available for a planar data in PPI scan) manifest a coarser mesh of $\sim 0.25D$ or 30 metres throughout the domain which is comparable to the coarser region of the LES mesh. However, a disparity in the temporal resolution between the LES and LIDAR resolutions are evident in the fact that the resolution of LES simulations is 0.06 secs, while that of the LIDAR retrieved scans $\sim 1-4$ minutes.

3. Results and Discussion

In this section we present a comparison of the temporally filtered LES and 2D VAR optimization based retrieval of LIDAR scan data. Figure 3 illustrates the snapshots (horizontal velocity magnitude) obtained by 2D-VAR retrieval algorithm around the bottom tip of the rotor from raw LIDAR data manifesting large scale structures at two different time-stamps, 6:13 am and 6:44 am. The snapshots show some high velocity large scale energetic structures near $y \sim$ 400 metres and 1200 metres. Some of those structures have completely dominant x directional flow, despite a prescribed mean wind direction. These might be attributed to the inaccuracy of the LIDAR retrieval schemes close to the azimuthal sweeping range of the scans. Hence, when subsequent comparison with the LES simulations have been performed later, we have extracted data in the inter-turbine regime in the spanwise direction (away from the periodic boundaries), with some discrepancies observed due to those high-velocity turbulent structures not captured by the LES simulations. Similar 0.5 minutes temporally filtered snapshots (5000 LES snapshot realizations) from the LES simulations are also documented in Figure 4 at the hub-height and bottom tip location of the wind turbines. Note, that the hub-height location of the turbines illustrates some turbine-wake foot-prints not conspicuously observed at the bottom tip. The temporal filtering is performed to remove noise from the instantanous horizontal velocity snapshots facilitating the attempt to compare with the field experimental results. Additionally, the temporal filtering of 0.5 and 2 minutes corresponds to $\sim 1/4$ and a full eddy turn-over time H/U_{hub} (corresponding to a hub-height velocity) respectively. Consequently the temporal filtering ensures that the circulations of large scales in the vertical direction is filtered retaining only variations larger than the 2 min time scale.

To complement the above plots, Figure 5, manifests the snapshots of instantaneous horizontal velocity magnitude, (timestamp of $6:13$ am and $6:44$ am) at the bottom tip location of the wind turbines. It is clear that due to the noise present in the instantaneous snapshots capturing turbulence, the wakes are not as prominently visible as they are in the temporally filtered snapshots (0.5 minutes filtered LES data in Figure 4).

Additionally, in Figure 6 we document the instantaneous vertical velocity captured by the LES simulations. In particular, Figure 6a illustrates the z variation of vertical velocity at 6:13 am just behind the second row of turbines, while Figure 6b shows the vertical velocity at the bottom tip of the rotors at 6:13 am. Note that the 2D-VAR retrieval scheme, essentially retrieves only in-plane horizontal velocities from the low elevation angle PPI scan, thus neglecting the vertical velocity effects. This is a reasonable approximation, since even though the vertical velocity at the outer layer contains large structures ($w \sim$ 15-20% of horizontal velocity magnitude) depicted by LES simulations, near the bottom tip of the rotor, the vertical velocity is $\lesssim 5\%$ of the horizontal velocity magnitude with some small-scale energetic bursts corresponding to $\sim 20\%$ of the horizontal velocity dispersed throughout the xy plane (See Figure 6b).

Figure 7 depict the comparison of temporally filtered LES simulations with LIDAR retrieval (time filtered) between the turbines T3 and T7 and 400 metres upstream of it for 2 different temporal snapshots 6:13 am and 6:44 am. Interestingly, the plots depict some agreement within

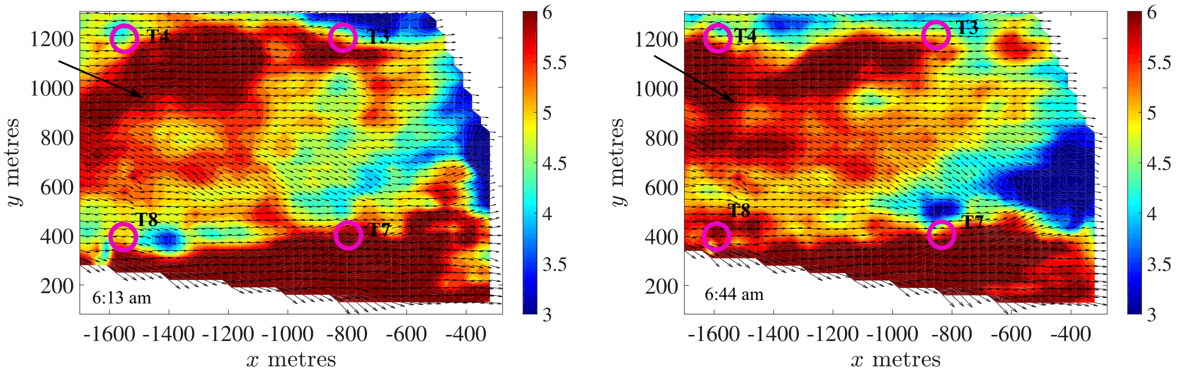

(a) (b)

Figure 3: Snapshot of horizontal velocity magnitude $\sqrt{u^2+v^2}$ m/s for flow past the wind farm obtained from the retrieval of LIDAR scan data using 2D VAR algorithm. z location at the bottom tip of the rotor. LIDAR data collected on 31st August 2016. Arrow – direction of mean wind; Magenta circles: Location of turbines

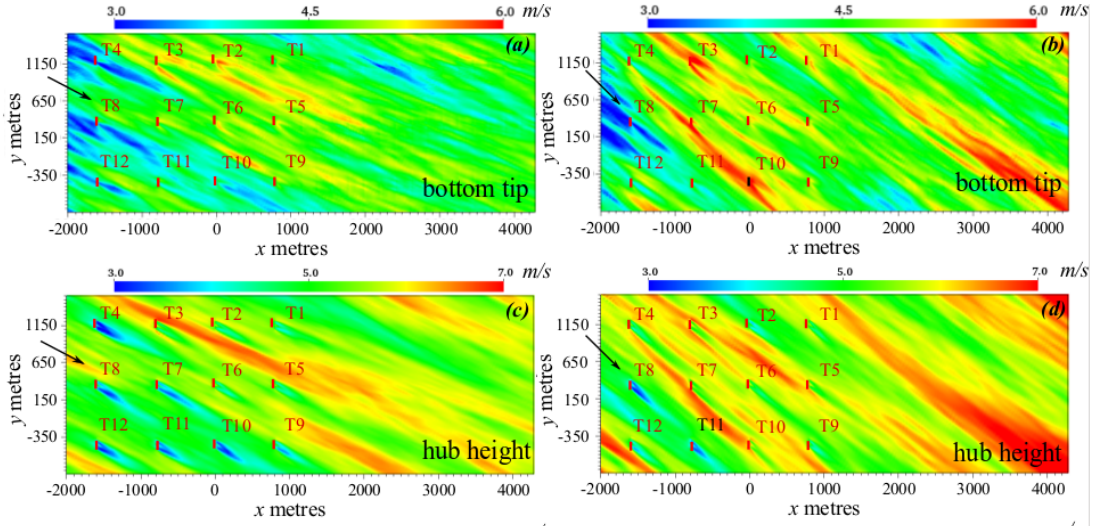

Figure 4: Horizontal velocity magnitude $\sqrt{u^2+v^2}$ in m/s in the xy plane from the LES data temporally filtered for 0.5 minutes. Timestamp location: (a), (c) – 6:13 am, (b), (d) – 6:44 am. Arrows - Mean wind direction.

a band of spatial uncertainty of the vertical locations z, even though some discrepancies could be noted possibily due to the inability of the LES model to capture the high velocity structures which might arise either from geophysical effects/atmospheric instability not modeled by the simulations or the inaccuracy of the LIDAR retrieval schemes near the maximum and minimum range of the azimuthal scans. At this point, due to lack of enough data, the reason of those high velocity structures in LIDAR scans is not clearly understood and requires further investigation.

In Figure 8 temporal evolution of the spatially filtered horizontal velocity magnitude (instantaneous, time-filtered for 0.5, 2 mins – integrated in between the line-region of two turbines T3-T7) has been depicted. Interestingly, the temporal variation of 2 min filtered LES data closely follows the mean wind fed to the simulation through the precursor ABL. The figure further illustrates that the temporal variation of LES simulation data is within the bounds of

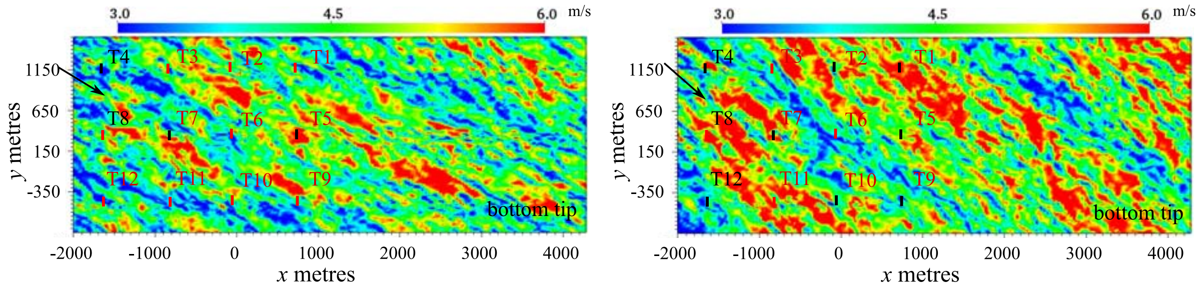

(a) (b)

Figure 5: Instantaneous horizontal velocity magnitude $\sqrt{u^2+v^2}$ in m/s taken from the LES data in the xy plane. Timestamp location: (a) – 6:13 am, (b) – 6:44 am.

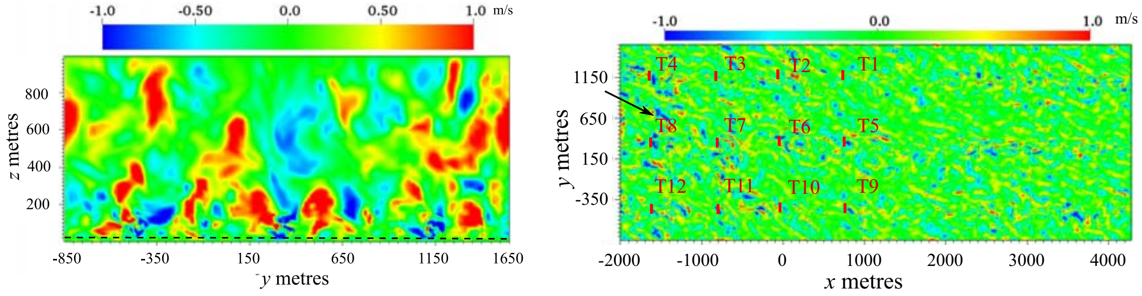

(a) (b)

Figure 6: Instantaneous snapshots of vertical velocity w in m/s taken from the LES data at (a) yz plane at $x = x_t + 0.5D$ (x_t, location of second row of turbines). Dashed line at $z = z_h - D/2$. (b) xy plane at $z = z_h - D/2$. Data collected at timestamp of 6:13 am.

variability of the LIDAR retrieved scans capturing some temporal trends from the LIDAR data.

Figure 9 depict the spatially averaged streamwise and spanwise u, v and w energy spectra for two different time-stamps, 6:13 am and 6:44 am. The spectra indicates that the Kolmogorov $-5/3$ scaling is produced at scales $\approx D$. The different timestamp plots indicate that the smaller scales $\sim O(D)$ of the spectra converge quickly towards the $-5/3$ cascade ($\lambda_{x,y}^{2/3}$ for premultiplied spectra in wavelengths) due to small eddy turn over times, but the large scales $\gtrsim O(10D)$ do not hint towards a trend due to the massive eddy turn over times. Note, that a premultiplied spectra in the log-log scaling has been used to reduce the differences in the energy content artificially at different length scales, making the plot compact, and for the advantage of illustrating the power-law scaling using slope of the lines. The u and v energy spectra in the current flow are much larger than their wall normal w counterpart except perhaps at scales $\lambda_{x,y} \lesssim D$. While for spanwise spectra (λ_y direction), the spectral content of u energy is always greater than the v counterpart, for the streamwise spectra (λ_x direction), a threshold scale exists ($\sim 7D$), below which the v spectra is dominant.

4. Conclusion and Future Work

In the present chapter we have proposed an LES methodogy for the flow past the wind farms using atmospheric boundary layer precursor inflow driven by variable mass flux and wind direction obtained from a cup and vane anemometer data during a LIDAR field experimental campaign. The methodology serves as an important step towards fundamental understanding of the realistic flows past large wind farms. The LES results have been compared against the

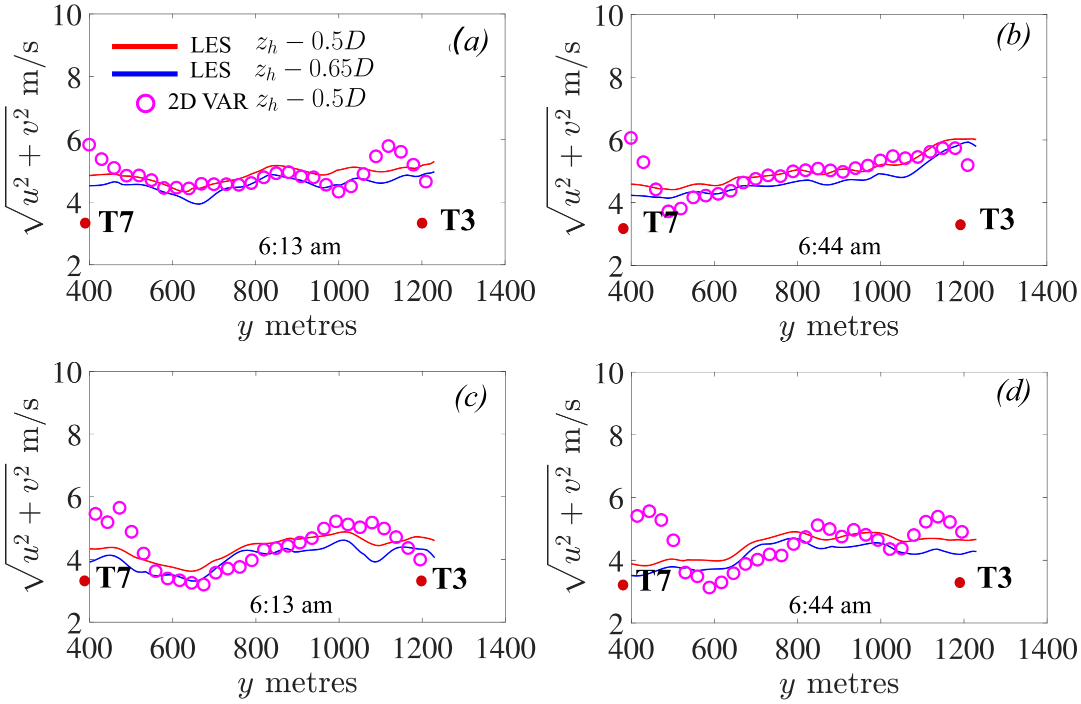

Figure 7: Comparison of 2 min. filtered LES and LIDAR scan experiments. Estimated location of turbines T7 (left), T3 (right) marked in red circles. LIDAR data collected at 31st August 2016, start time – 6:13 am & 6:44 am from which temporal filtering started. (a), (b) – Turbine locations T3 to T7, (c), (d) 400 metres upstream of turbine locations T3 to T7.

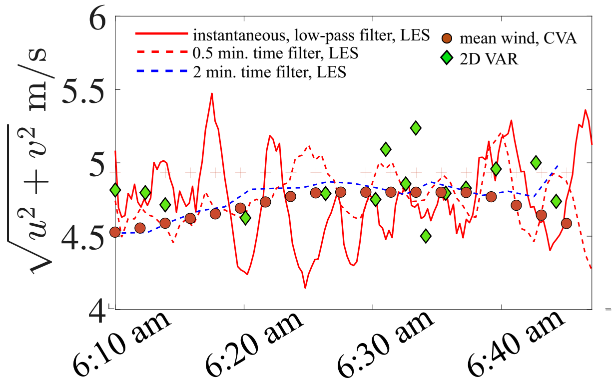

Figure 8: Temporal variation time-filtered horizontal velocity magnitude spatially integrated in the spanwise direction between turbine locations T3 and T7. Instantaneous data is low-pass filtered (5 point moving average filter) to illustrate the large scale trends. All data collected/calculated at $z = z_h - D/2$.

LIDAR field experimental data (retrieved using a 2D VAR algorithm [20]) reconstructing the horizontal velocities (u, v) near the bottom tip of the rotor. Both the temporally filtered data at the inter-turbine spatial location as well as the temporal evolution of the spatially filtered data in LES and LIDAR scans lie wihin comparable bounds, despite some discrepancies in their trends. These differences are attributed to the uncertainties in measuring locations, stability of ABL and large scale variations imposed by the geophysical effects not considered in our neutral LES simulation with near-wall modelling driven by the mean wind.

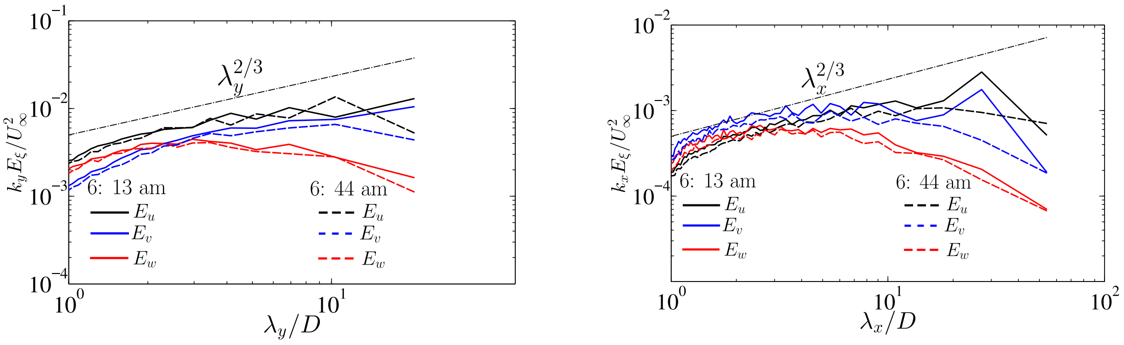

(a) (b)

Figure 9: Instantaneous snapshots of streamwise/spanwise energy spectra of LES data averaged in the spanwise/streamwise, wall-normal direction.

Presently, the LES model is designed in a neutral framework. We would further extend its capability towards handling stably stratified and convectively unstable boundary layers to facilitate comparison at other timestamps where stratification of the boundary layers would play a conspicuous role. As a final remark, the discrepancies observed between the LIDAR retrieval results and the LES simulations driven by realistic mean wind and attributed to the inability of LES to capture some large scale structures, indicates towards a potential need of data assimilation, i.e. coupling the instantaneous LIDAR retrieval fields (as a function of space and time) to the coarse LES (or WRF) precursor simulations for capturing more realistic time-resolved flow structures past the wind farm.

References

[1] Porté-Agel F, Wu Y T and Chen C H 2013 *Energies* **6** 5297–5313
[2] Munters W, Meneveau C and Meyers J 2016 *Boundary-Layer Meteorol.* **159** 305–328
[3] Choukulkar A *et al.* 2017 *Atmos. Meas. Tech.* **10** 247–264
[4] Wu Y T and Porté-Agel F 2011 *Boundary Layer Metereol* **138** 345–366
[5] Chamorro L P and Porté-Agel F 2011 *Energies* **4** 1916–1936
[6] Lungo G V 2016 *Journal of Wind Engineering and Industrial Aerodynamics* **149** 35–39
[7] YYCheng W, Liu Y, JBourgeois A, Wu Y and EllenHaupt S 2016 *Phil. Trans. R. Soc. A.* **375** 2016103
[8] Monache L D *et al.* Ensemble-based data assimilation for wind energy predictions The fifth international symposium on computational wind engineering (cwe2010) chapel Hill, North Carolina, USA May 23-27, 2010
[9] YYCheng W, Liu Y, JBourgeois A, Wu Y and EllenHaupt S 2017 *Renewable Energy* **107** 340–351
[10] Castro F A, Santos C S and da Costa J C L 2015 *Wind Energ.* **18** 1251 – 1272
[11] Mirocha J D *et al.* 2015 *Journal of Renewable and Sustainable Energy* **7** 043143
[12] Risan A, Lund J A, Chang C Y and Saetran L 2018 *Remote Sens.* **10** 59
[13] Chatterjee T, Cherukuru N W, Peet Y and Calhoun R J 2017 Incorporating realistic geophysical effects of mean wind from lidar measurements in large eddy simulation of wind turbine arrays AIAA paper 2017–1165
[14] Chatterjee T and Peet Y T 2017 *Physics of Fluids* **29** 075175
[15] Rajamani B 2008 *Hybrid RANS-LES modeling of high Re turbulent flows* Ph.D. thesis University of California, Los Angeles
[16] Chatterjee T and Peet Y 2016 Large eddy simulation of a 3 × 3 wind turbine array using actuator line model with spectral elements AIAA paper 2016–1988 04 - 8 January 2016, San Diego, California
[17] Chatterjee T and Peet Y T 2018 *Physical Review Fluids* **3** 034601
[18] Wu Y T and Porté-Agel F 2015 *Renewable Energies* **75** 945–955
[19] Munters W, Meneveau C and Meyers J 2016 *Phys. Fluids.* **25** 025112
[20] Cherukuru N W, Calhoun R J, Krishnamurthy R, Benny S, Reuder J and Flugge M 2017 *Energy Procedia* **137** 497–504